

# TESTING AND SIMULATION OF DAMAGE GROWTH AT PLY DROPS IN WIND TURBINE BLADE LAMINATES

Pancasatya Agastra and John F. Mandell  
Department of Chemical and Biological Engineering  
Montana State University – Bozeman  
Bozeman, MT 59715

## ABSTRACT

Wind turbine blades are typified by thick, resin-infused laminates containing ply drops for thickness tapering. A complex structured test coupon has been developed to represent a simplified version of the substructure around ply drops; the coupon is relatively easy to fabricate and test, including tension, reversed and compression loading in fatigue [1,2]. This coupon is used to compare the performance of five types of resin, and several fabrics and ply drop geometries. The effects of these variables on damage growth are quantified for static and fatigue loading, showing significant effects of the resin. Resin types included in this study are polyester (UP), toughened and un-toughened vinyl ester (VE), epoxy (EP) and polydicyclopentadiene (pDCPD).

The strain energy release rates for delamination under pure Modes I and II, and mixed-mode have also been determined using established test methods, as have the in-plane static and fatigue properties. Based on the geometry and in-plane and interlaminar properties, a simulation of the damage growth under static loading has been developed using ANSYS finite element modeling. Simulation results are consistent with the experimental damage growth results, and are helpful in relating the performance back to more fundamental properties such as the pure and mixed mode delamination tests, and, in turn, to resin properties. The simulation study also identifies parameters to which ply drop delamination resistance is sensitive, including: variations in elastic constants related to fiber content variations, assumed and actual boundary conditions, ply resin cracking in biax plies and representation of pure and mixed mode delamination data.

## 1. INTRODUCTION

Wind turbine blades are complex composite structures containing a variety of structural details which can compromise blade performance. Local material properties are affected by variations in fiber content and alignment. Geometric features and material discontinuities as in materials transition areas complicate local stress fields, often introducing significant third-dimensional stresses which can lead to ply delamination. Resin selection for blades has generally been focused on performance in relatively simple laminate coupons with reinforcing fabrics and process parameters representative of blade manufacturing by resin infusion. The approach used in this program has been to develop a test coupon which is representative of the more complex structural details in blade construction, where resin dominated failures occur in service, and

which is still relatively inexpensive to fabricate and test compared to full blade substructure tests [1,2]. This allows the evaluation of multiple resin options in a realistic structural context.

A ply drop is a structural detail integrated into the thick laminates of wind turbine blades to provide thickness tapering. Stress concentration arising at this structural detail can lead to ply delamination and loss of structural integrity [3,4]. Ply drops have been the subject of many studies in aerospace composite applications [5-6] as well as wind turbine blades [3, 7-9]. Standard tests cited later give the resistance to ply delamination,  $G_{Ic}$  and  $G_{IIc}$  for pure opening and shearing modes, which are a strong function of the resin toughness [1, 10]. In a composite structure the behavior is more complex than for simple pure mode delamination tests, with the controlling strain energy release rates following mixed opening and shearing modes, and depending on geometry and damage development such as matrix cracking in off-axis plies [1, 3]. While results from the test coupon can be interpreted directly in terms of knockdowns on allowable strains, finite element modeling is required to relate the structural response to more basic in-plane and interlaminar properties, which is the major objective of this paper.

Several variables affecting delamination at ply drops for thick fiberglass laminates have been explored in the experimental part of this work: resin and fabric types, ply drop thickness (number of individual plies dropped at a single position), applied load level, and damage growth under tensile, compressive, and reversed-loading in fatigue. Taken together, these represent a broad range of parameters commonly encountered in the wind turbine blade application [1].

Finite element modeling has been used both to design the test coupon and to simulate damage growth. Coupon design, reported in more detail in References 1 and 2, was focused on minimizing strain gradients across the thickness due to bending of the non-symmetric geometry. As indicated in Figure 1 for a case with two ply drops (total of 2.6 mm dropped unidirectional material), strains across the thickness on the thin side vary by less than 10% when grip lateral movement is effectively constrained. The low strain variation across the thickness allows the test results to be incorporated as a design strain knockdown, rather than requiring a fracture mechanics based design strategy.

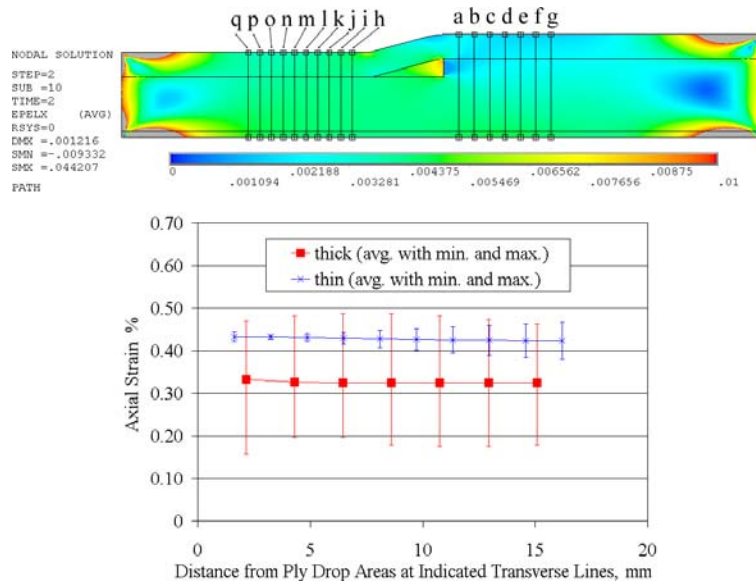


Figure 1. Axial strain distribution (top), and line plots across thickness at indicated axial locations from FEA for a tensile force of 44.5 kN [1, 2].

Simulation of damage growth based on experimental observations of damage geometry and basic materials properties has been carried out for static loading, with fatigue simulations to follow. Validated simulations are a key link in relating more basic material properties and geometric features to damage growth, and have been used successfully for delamination problems in composites [11].

## 2. EXPERIMENTATION

### 2.1 Materials

Laminates representing the separate components of the complex coupons were tested in addition to the complex coupon laminates containing ply drops. Three types of laminates were fabricated and tested:

- 1) Standard laminates. Unidirectional and biaxial laminates were tested to obtain ply input data and as baseline fatigue cases for comparison to the complex coupon results.
- 2) Delamination laminates. Unidirectional laminates with simulated starter cracks were used in standard delamination tests to obtain  $G_{Ic}$ ,  $G_{IIc}$  and mixed mode data for use in the simulations as well as basic resin comparisons.
- 3) Ply drop laminate. Multidirectional laminates with ply drops for complex coupons.

All laminates were manufactured using vacuum bag resin infusion as summarized in Figure 2. The vacuum bag components are given in Table 1. The aluminum mold was coated with mold release prior to laying up the components. Vacuum pressure of ~640 mm Hg was applied prior to injection to hold everything in place. Table 2 gives the resins and post cure temperatures and Table 3 gives the E-glass reinforcing fabrics. The pDCPD is a new type of thermoset infusion resin with high toughness and low viscosity [1,12]. Standard laminates without ply drops used

flow media on the top only; delamination laminates used an added caul plate on top and flow media top and bottom, with Nylon film crack starter strips; and the complex coupon laminates included ply drops in the top uni fabric plies, under the surfacing biax plies (Figure 2). A typical ply drop panel with four plies dropped at the same location is shown in Figure 3, and cross-sections of the complex coupons with the two different biax fabric are shown in Figure 4.; note that the unidirectional Vectroply fabric actually contains a small amount of 90° strand as backing (Table 3), so that the ply is designated as 0/90. Reference 1 gives local fiber contents corresponding to Figure 4, used in the simulations.

The resin and its components were mixed according to the manufacturer's recommendation. To minimize micro bubble introduction, a special impeller for viscous resin Jiffy Mixer LS-1 and mixing speed was kept at 300 RPM for 2.6 L resin, and 500 RPM for 4.3 L. Mixing time was five minutes, with an additional five minutes at rest to remove entrapped air bubbles. Injection time varied from 3-15 minutes, depending on the size of the laminates. Laminates were infused at room temperature maintained at ~18°C, cured at this temperature for 24 hours, and postcured for another 24 hours at a prescribed temperature summarized in Table 2.

## 2.2 Test methods

The complex laminate coupon with ply drops is shown in Figure 5. The development of this specimen geometry has been described elsewhere [1,2]; Figure 1 indicates the relatively uniform strain field despite the non-symmetry of the geometry. A composite tab was bonded to the thin side of the specimen to level the thickness. The faces to be gripped were then trimmed to a flat and level condition. Thickness and width were measured at 25 mm away from the edge of ply drop on the thin and thick sections. The non-symmetrical complex coupon requires specialized lateral constraint on the hydraulic grips [1].

Complex coupons with ply drops were tested statically and under fatigue loading at three different R-values, R=0.1 (tensile), R=10 (compressive), and R=-1 (reverse loading), where R is the ratio of minimum to maximum load. Delamination specimens were tested for mode-I, mode-II, and mixed-mode delamination, under displacement control 1.5mm/min. Figure 6 gives mixed mode geometry and test apparatus schematics [13,14]. These tests follow the ASTM standards with minor modifications: ASTM D5528 for mode I and D6671 for mixed mode; the end notched flexure test was used for mode II [1]. Fatigue test frequency was controlled so that the temperature would not exceed 5°C higher than room temperature. Test specimen surfaces were cooled with a fan. Further test details can be found in Reference 1.

Static testing for the complex coupon specimen was in tension. The load was increased incrementally and crack lengths were measured at each step, until crack length L1 reached the grip. Figure 7 is a schematic of the damage geometry which was typical for all cases.

Table 1 Molding materials

Mold	Aluminum 6061 plate, 61 cm × 90 cm × 12.7 mm
Mold Release	Loctite Frekote 44-NC Mold Release Agent
Release Ply	Airtech Release Ply Super F, at top and bottom of laminate
Flow Media	Airtech Greenflow 75, two layers, and 9.5mm-ID Polyethylene spiral wrap
Vacuum Bag	Airtech Vacuum Bag Wrightlon 7400, 76µm thick
Tacky Tape	Airtech AT-200Y
Crack Starter	Richmond Aircraft Products, Inc. VAC-PAK® HS 8171-6 Co-Extruded High Temperature, Nylon 6 Film, 50µm thick

Table 2. Resin type and post cure schedule

Resin Type	Resin	24-hr Post Cure Temp.
Epoxy EP-1	Hexion MGS RIMR 135/MGS RIMH 1366	90°C
Polyester UP-1	U-Pica/Hexion TR-1 with 1.5% MEKP	90°C
Vinyl ester VE-1	Ashland Derakane Momentum 411-350 with 0.1% CoNap, 1.0% MEKP, and 0.02 phr 2,4-Pentanedione	100°C
Toughened vinyl ester, VE-2 FIX	Ashland Derakane 8084 with 0.3% CoNap and 1.5% MEKP	90°C
pDCPD (poly-Dicyclopentadiene)	Materia Inc.	N/A

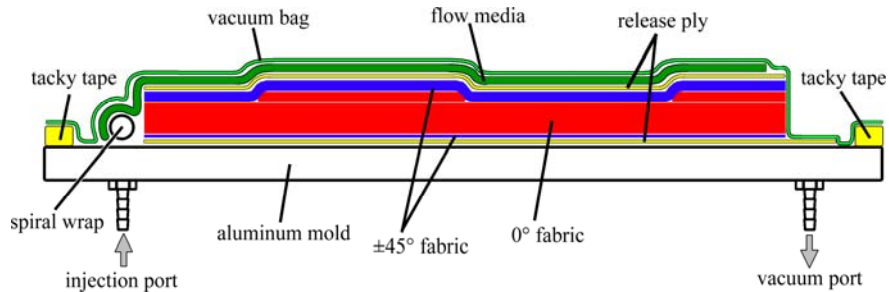


Figure 2. Infusion processing of laminates with ply drops

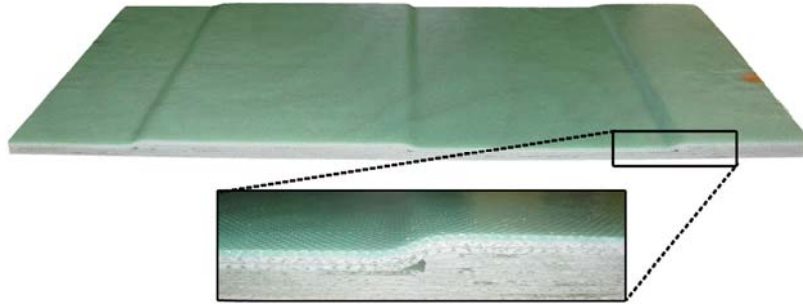


Figure 3. Typical ply drop laminate panel with four plies dropped at single locations [1,2] (showing flow media on top)

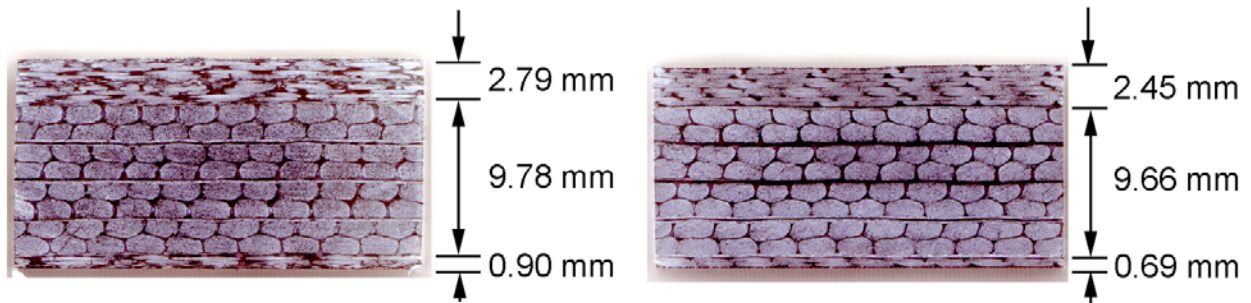


Figure 4. Cross-sections (sectioned at 90°) of complex laminates with two ply drops, thick side, layup from top surface  $[(\pm 45)_4/(90/0/0/90)_4/(\pm 45)]$ ; Fabric M  $\pm 45$ 's (left), Fabric L  $\pm 45$ 's (right).

Table 3. Fabric Definition

Fabric Type	Manufacturer and Designation	Fiber Areal Weight, g/m <sup>2</sup>						
		Total	0°	90°	-45°	+45°	mat	stitch
Unidir. 0/90 (Fabric D)	Vectorply E-LT-5500	1875	1728	114	0	0	0	33
Biaxial $\pm 45$ (Fabric M)	Fiber Glass Ind. (FGI) SX-1708	847	0	0	292	292	258	6
Biaxial $\pm 45$ (Fabric L)	Saertex VU-90079-00830- 01270-000000	829	0	21	401	401	0	6

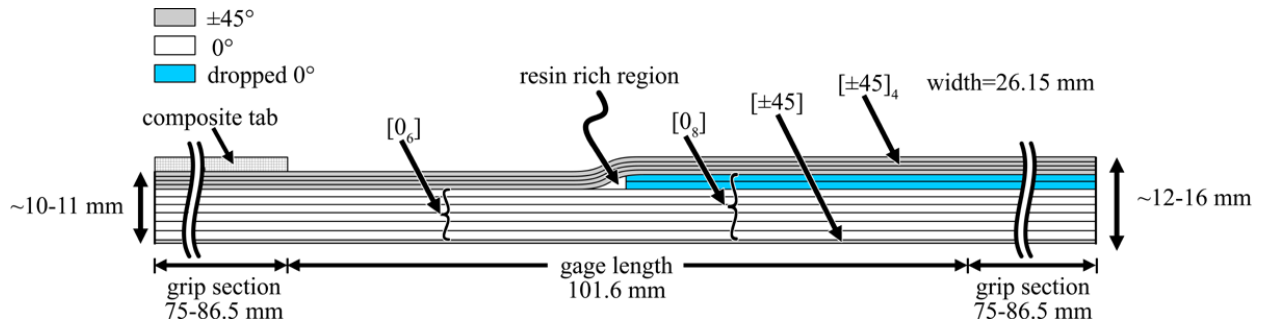


Figure 5. Complex coupon geometry [1,2]

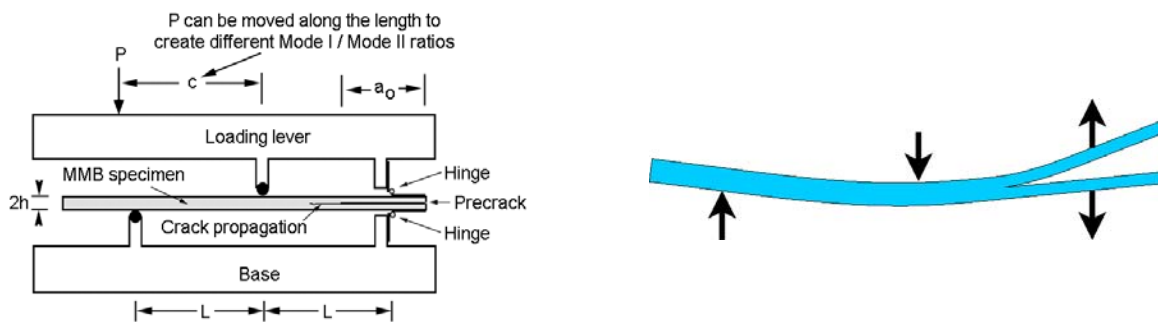


Figure 6. Mixed mode I and II delamination test geometry

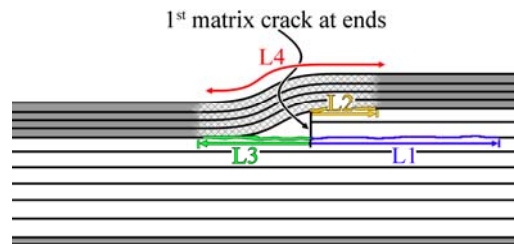


Figure 7. Damage geometry, where L1, L2, and L3 are delamination cracks and L4 is distributed matrix cracking in the biax plies (adapted from References 1 and 2)

### 3. SIMULATION

#### 3.1 Simulation Input

The simulation input was based on experimental data for crack geometry (Figure 7) and material properties either given here or in Reference 1. Observed complex coupon details were included in the model (Figure 8):

- A. Curvature of the overlaying top plies.
- B. Simplification of the junction between the  $\pm 45^\circ$  and the  $0^\circ$  layer
- C. Compaction at the top of the ply drop edge
- D. Resin rich region

Initial simulations reported here assumed crack lengths for L2 and L3 (Figure 7) as 3 mm for higher values of L1 as discussed later. Softening due to the matrix cracking in the biax plies (L4) was included through a multi-linear elastic stress-strain curve, Figure 9, synthesized from experimental stress-strain curves for fabric M with resins EP-1 and UP-1, which gave nearly identical results [1]. The length of the primary delamination, L1, was assumed in the simulation, and the load to achieve the mixed mode failure criterion was determined. Convergence was difficult when biax modulus changes were included, and this feature was deleted from many runs to reduce run times.

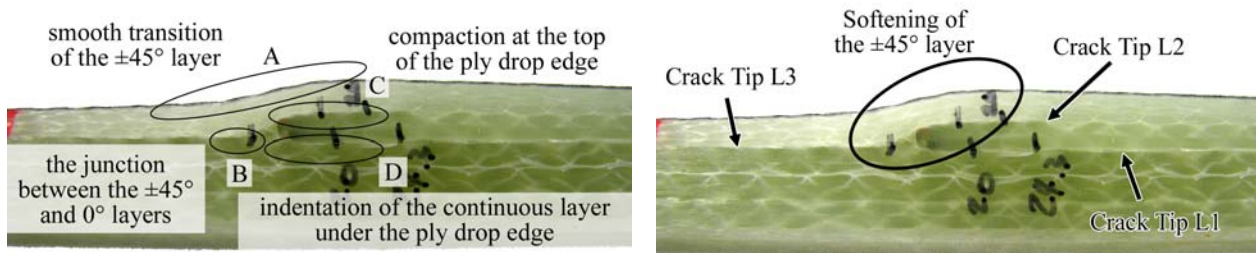


Figure 8. Ply drop details for the simulation.

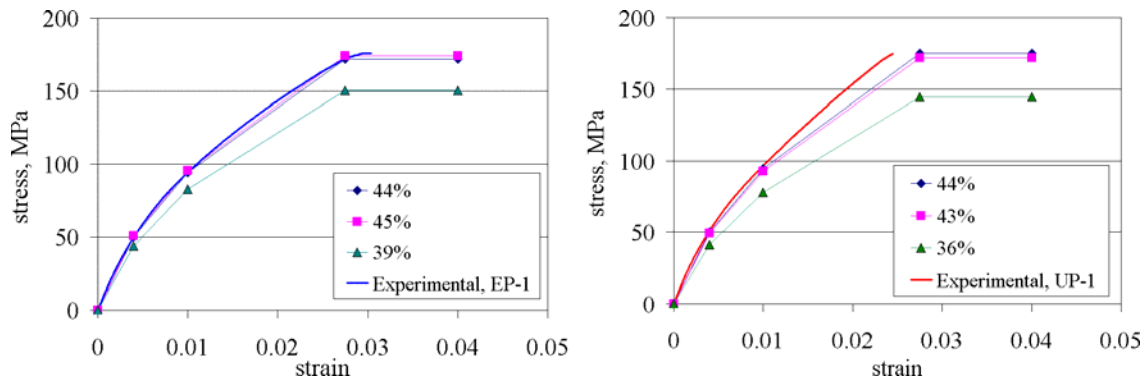


Figure 9. Multi-linear elastic tensile stress-strain curve for biax fabric M for EP-1 (left) and UP-1 (right)

### 3.2 Material Properties and Geometry

Figure 10 gives typical element meshes with coordinate systems and material domains. The FEA used ANSYS PLANE82 elements with contact elements (0-friction) on crack surfaces. The elements around the crack tips were sized according to ANSYS recommendation.

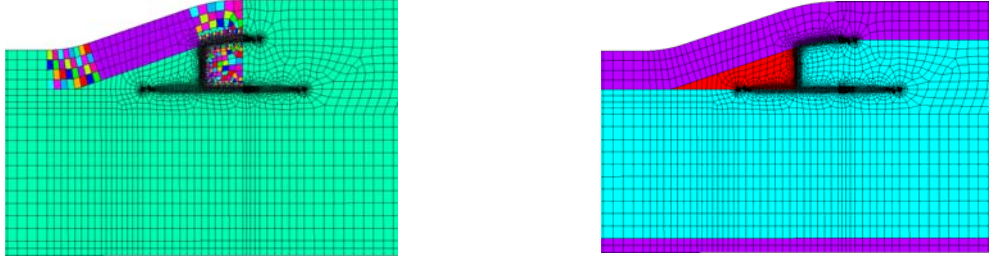


Figure 10. Finite element model details around the crack tips (left: rotated coordinate system; right: material domains)

The orthotropic material properties were taken from Reference 1, adjusted for local fiber content variations in particular plies [1] or were estimated from similar materials [3] where not available. Crack fronts were modeled and the strain energy release rates were calculated using the one-step VCCT method [15].

Table 4. Material Properties for FE simulation (\*estimated properties from [3]).

Material Properties	Fabric D 0°	Fabric L ±45	Fabric M ±45	Epoxy Neat Resin
Fiber Volume Content	0.54	0.51	0.44	0
$E_x$ , GPa	41.80	13.80	13.60	3.20
$E_y$ , GPa	7.38*	7.52*	7.52*	X
$E_z$ , GPa	14.00	11.80	13.30	
$G_{xy}$ , GPa	2.63*	2.83*	2.83*	
$G_{yz}$ , GPa	2.63*	2.83*	2.83*	
$G_{xz}$ , GPa	2.63	9.24	11.8	
Density, kg/m <sup>3</sup>	1924*	1884*	1788*	1190
$\nu_{xy}$	0.280*	0.264*	0.264*	X
$\nu_{yz}$	0.280*	0.381*	0.381*	
$\nu_{xz}$	0.280	0.51	0.55	

### 3.3 Delamination Criterion

Mixed mode ply delamination is the dominant feature of ply drop behavior. Figure 11 gives typical mixed mode data for two unidirectional fabrics at two fiber content ranges, for three resin types: epoxy (EP), vinyl ester (VE), and unsaturated polyester (UP), from Reference [1], where particular resins and fabrics are identified (fabric D is described in Table 2). The general shape of the mixed mode failure criterion follows that described by Reeder and Crews [13], as related to disruption of planar mode I cracks by hackle formation from the mode II component. Thus, a

mode II component allows  $G_I$  to increase above the pure mode  $G_{Ic}$  value. The pure and mixed mode toughness increases for increasing neat resin toughness and decreasing fiber content [11]. Tough resins such as toughened epoxies and thermoplastics, or pDCPD, tend to a linear relationship between  $G_I$  and  $G_{II}$  as [16]:

$$G_I/G_{Ic} + G_{II}/G_{IIc} = 1 \quad [1]$$

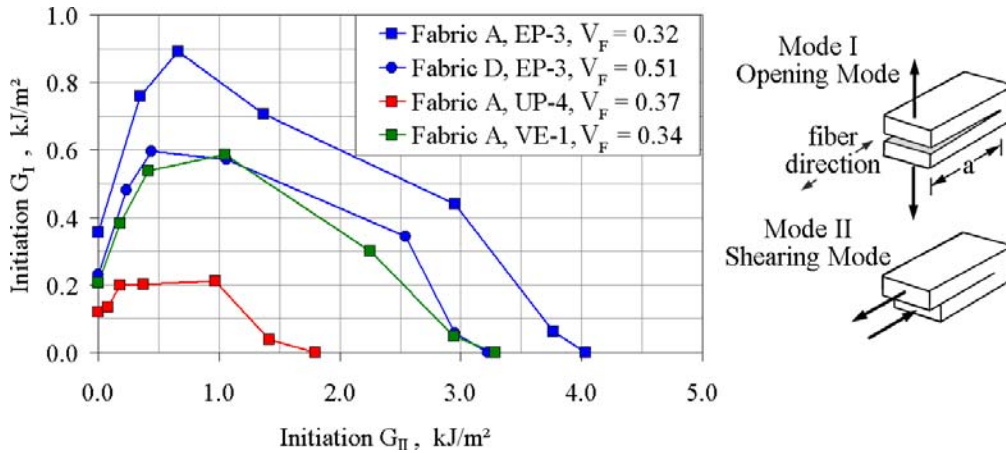


Figure 11. Mixed mode delamination results for various resin types and fiber contents [1,15].

## 4. RESULTS

### 4.1 Experimental

#### 4.1.1 Delamination Tests

Pure mode critical strain energy release rates for the various resins with Fabric D are given in Table 5. The  $G$  values are calculated for initial crack growth from the Nylon film using the 5% offset method described elsewhere [1, 3]. Consistent with Figure 11, the general ordering of toughness from low to high is polyester, vinyl ester and epoxy, as reported earlier [1-3], the differences between resins are significant. The Vectorply ELT 5500 fabric (D) contains a small amount of  $90^\circ$  backing strands on the side referenced as 90, so the delamination interface could be 0/0, 90/90 or 0/90. Table 5 contains toughness values for 0/0 and 90/90 only; toughness values are generally higher for the 0/0 interface, where the  $0^\circ$  strands nest, than on the straighter 90/90 interface (Figure 4). The irregular 90 face of the fabric, with occasional backing strands, results in high scatter for this interface. The primary delamination for the complex coupon, L1 (Figure 7), is on a 90/90 interface for the layup used in that test. The results in Table 6 also indicate that the toughened vinyl ester, VE-2, reaches similar toughness levels to the epoxy. Also notable is the pDCPD resin, which is ductile in behavior, and reaches very high  $G_{Ic}$  levels, similar to highly toughened epoxy or thermoplastic resin laminates like PEEK [16,17]; only the 0/0 interface has been tested for the pDCPD resin. Use of initiation values for  $G_{Ic}$  results in the lowest value for infused fabrics of this type; as the crack extends, mechanisms like fiber bridging can significantly raise the critical  $G_I$  value by several times the initial value, with stronger effects seen for the more brittle resins like polyesters [3]. Mixed mode data for the Fabric D laminates

with epoxy EP-1 and polyester UP-1 are given in Figure 12. This figure also illustrates the mixed mode failure criterion used in the simulations.

Table 5. Pure mode delamination test results. (Numbers in parenthesis are standard deviations for 3-5 tests.)

Resin	0-0 Interface				90-90 Interface			
	V <sub>F</sub> , %	Initial G <sub>IC</sub> , J/m <sup>2</sup>	V <sub>F</sub> , %	Initial G <sub>IIc</sub> , J/m <sup>2</sup>	V <sub>F</sub> , %	Initial G <sub>IC</sub> , J/m <sup>2</sup>	V <sub>F</sub> , %	Initial G <sub>IIc</sub> , J/m <sup>2</sup>
EP-1	60	303 (40)	60	3446 (201)	62	321 (38)	61	1887 (97)
UP-1	60	166 (17)	60	1662 (200)	62	175 (27)	62	928 (353)
VE-1	64	252 (24)	63	2592 (130)	64	223 (13)	63	1653 (124)
VE-2	61	433 (53)	61	2998 (313)	61	272 (33)	61	1689 (349)
pDCPD	64	1560(241)	64	2728 (305)	---	---	---	---

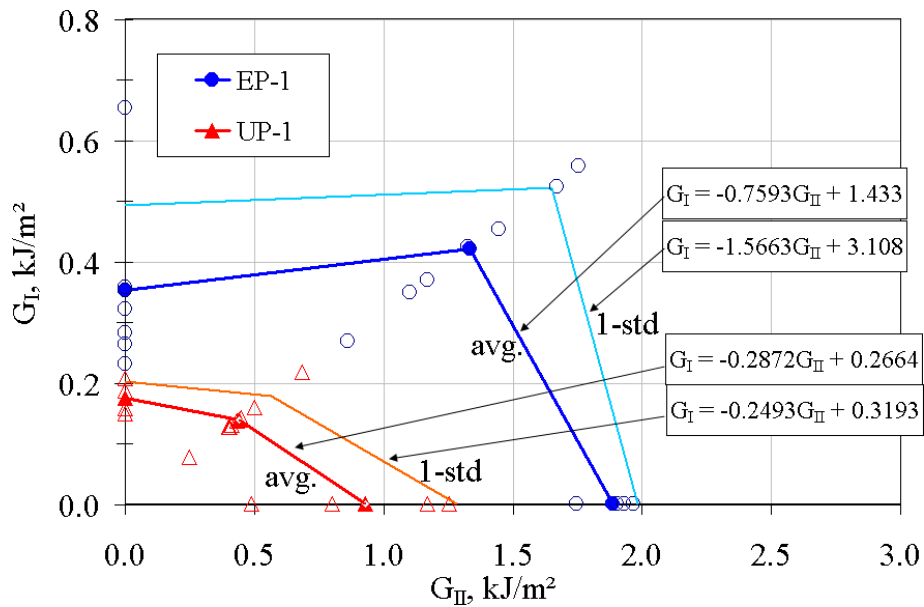


Figure 12. Mixed mode results for EP-1 and UP-1 resins, fabric D unidirectional laminates, crack positioned on the 90/90 interface, showing delamination criteria assumed in simulations

#### 4.1.2 Complex Coupon Static Tests

Figures 13 and 14 give comparisons of the delamination growth curves for the various resins [1]. The results in Figure 13, for biax Fabric M with unidirectional Fabric D, show the same ordering by resin as Figure 11 and Table 5: epoxy, vinyl ester and polyester, from highest to lowest. Load levels are reduced in Figure 14 for the baseline epoxy, EP-1, using the lighter biax Fabric L, which does not contain mat. The pDCPD resin outperforms the epoxy for the longer cracks, where the G<sub>I</sub> component becomes significant, as shown later. The last growth step (highest load) is unstable, so the final point shown represents the highest stable load achieved, but the crack length plotted is the value at crack arrest due to the grips.

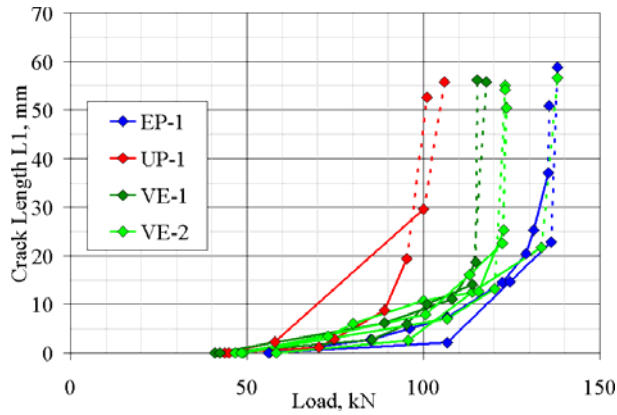


Figure 13. Static ply drop results for delamination growth, L1, vs. load, various resins, two plies dropped, fabrics M and D.

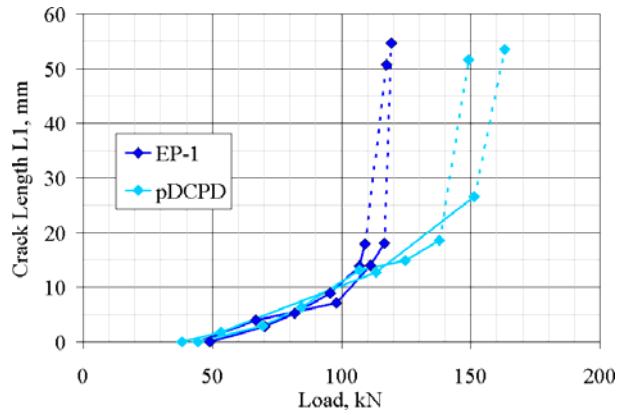


Figure 14. Comparison of epoxy and pDCPD under static loading, two plies dropped, fabrics L and D.

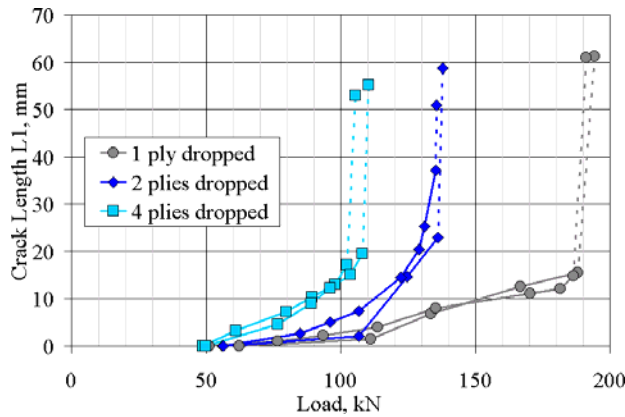


Figure 15. Effect of number of plies dropped, static tension, fabrics D and M, epoxy EP-1

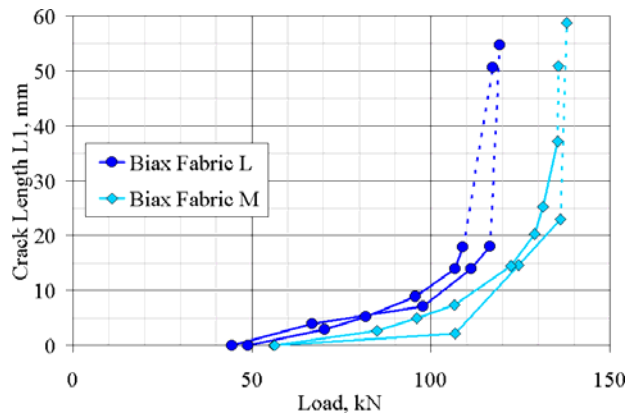


Figure 16. Effect of biax fabrics L vs. M with unidirectional fabric D and epoxy EP-1, two plies dropped

Figures 15 and 16 show the effects of the number of plies dropped at the single location, where the total thickness dropped is approximately 1.3 mm/ply. A strong effect of the dropped thickness is evident in Figure 15, as predicted [1]. One result of Figures 14-16 and the corresponding fatigue results is that thickness tapering can be more rapid for the tougher resins, to achieve similar static or fatigue delamination resistance [1,2]. The results depend on the types and number of plies of fabrics used in addition to the resin effects. The lighter biax fabric L results in delamination at lower loads than fabric M, which has an added layer of mat.

#### 4.1.3 Fatigue Results

Typical tensile fatigue results ( $R = 0.1$ ) for resin and geometric variations in Figures 16 and 17 show effects which correspond to the respective static Figures 13 and 15. Figure 18 compares epoxy EP-1 with pDCPD under reversed loading fatigue ( $R = -1$ , the most severe case) at three maximum load levels, and Figure 19 gives the corresponding delamination crack growth rates. The pDCPD shows increasing advantage in fatigue at lower loads and longer lifetimes more representative of the wind blade loading environment. Many other static and fatigue results can be found in References 1 and 2.

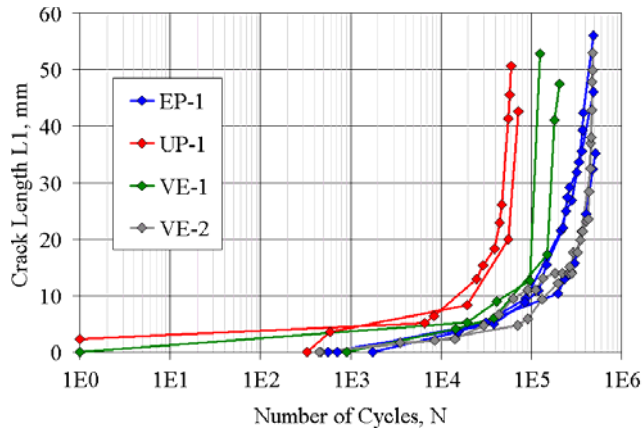


Figure 16. Fatigue test results with  $R=0.1$  at 44.5 kN maximum load for various resins with two plies dropped, fabrics M and D

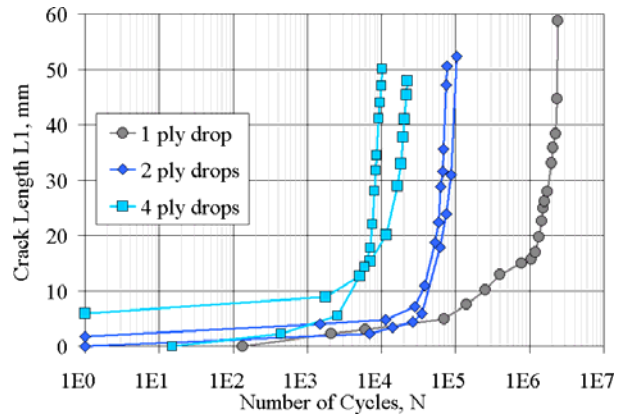


Figure 17. Effect of number of plies dropped on delamination growth in fatigue, resin EP-1, with a maximum load of 55.6 kN,  $R = 0.1$ , fabrics M and D.

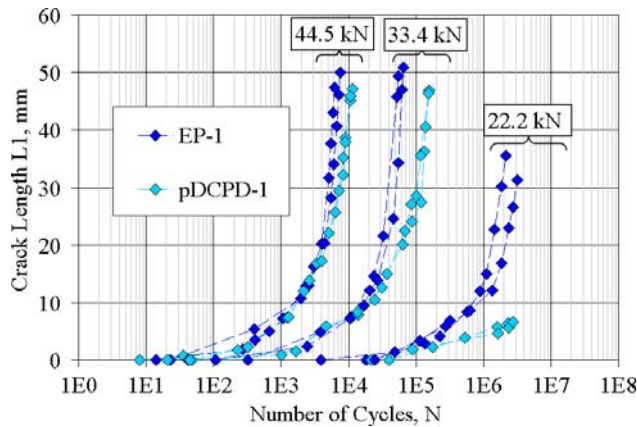


Figure 18. Epoxy and pDCPD under reversed loading  $R=-1$ , at various maximum load levels, fabrics L and D

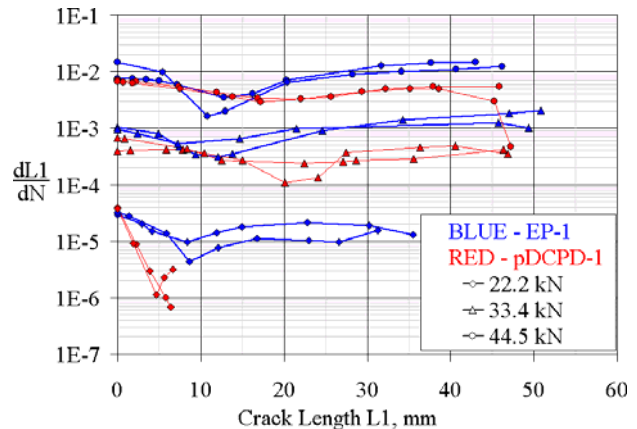


Figure 19. Crack growth rate,  $dL1/dN$ , vs. crack length for epoxy and pDCPD data in Figure 18

## 4.2 Simulation

Initial simulations have been carried out for static loading only, with resins EP-1 and UP-1 and fabrics D and M. Experimental results are given in Figure 13. The simulations were limited to the middle load and crack length ( $L1$ ) range, and, when included, assumed a length of about 3 mm for the secondary cracks  $L2$  and  $L3$  (Figure 7), which primarily extend further when  $L1$  becomes unstable. As noted earlier, softening of the biax plies was included in selected cases by using the multi-linear stress-strain curve in Figure 9. Early attempts at the simulation produced expected trends, but at significantly lower loads than found experimentally. Careful examination of the experimental setup showed slight lateral movement (at higher loads) of the grip due to the test coupon non-symmetry, before the grip constraint took full effect; lateral movement was on the order of one mm maximum. The boundary conditions were then modified to allow up to 1-mm lateral movement of the grip above 100 kN load (applying only to the epoxy resin). This modification significantly lowered the  $G_I$  and  $G_{II}$  values for a particular load and crack length,

raising the predicted loads to the range observed experimentally Figure 20 and Table 6). When free lateral movement was allowed the simulated loads were too high due to the reduced  $G_I$  and  $G_{II}$ . FEA values for  $G_I/G_{II}$  ratios in Figure 21 are generally similar to those found for prepreg ply drops by Wilson [18].

Figure 20 indicates good agreement between experimental data and simulated loads for the simulation parameters indicated. The difference between the epoxy and polyester resins is accurately represented by the simulation, primarily through the mixed mode failure criterion difference (Figure 12). Table 6 gives the sensitivity of the simulated loads at 15 mm delamination, L1. In addition to the parameters discussed above, predicted loads are increased by adjusting the failure criterion to the average value plus one standard deviation or adjusting the elastic constants to the measured in-situ ply fiber contents (from the listed values at a slightly lower fiber content), but decreased by the presence of secondary delaminations L2 and L3, or softening of the biax plies following Figure 9.

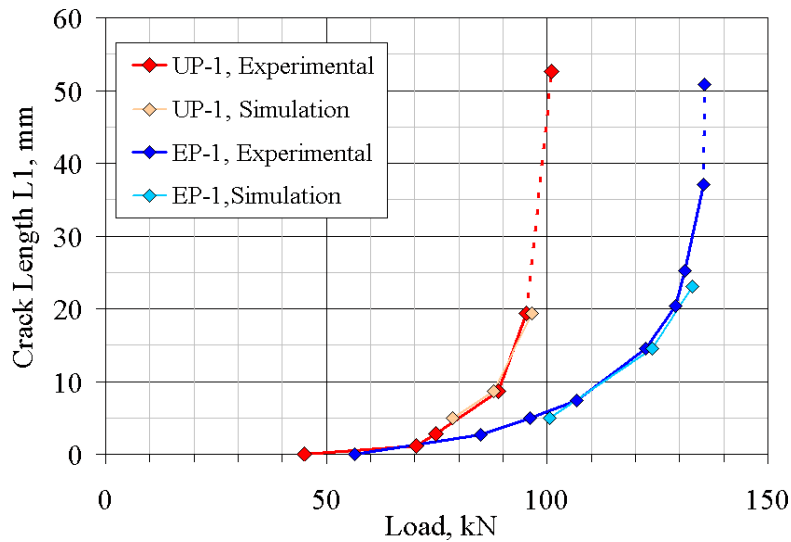


Figure 20. Simulated vs. experimental static tension results using the average mixed-mode failure criterion, 1 mm lateral displacement limit above 100 kN load, and no L2, L3 or biax softening

Table 6. Sensitivity results for resin EP-1 relative to standard case simulation

Mixed Mode Criterion	Lateral Movement Allowed	L2 and L3	E's Adjusted For $V_F$	Biax Softening	% Load Change at L1=15 mm
average	1 mm	0	yes	no	0 (std case)
average	free	0	yes	no	+19%
ave.+1 SD	free	0	yes	no	+26%
average	0 mm	0	yes	no	-15%
average	1 mm	3 mm	yes	no	-21%
average	1 mm	0	yes	yes	-24%
average	1 mm	0	no	no	-3%
average	0 mm	3 mm	no	yes	-22%

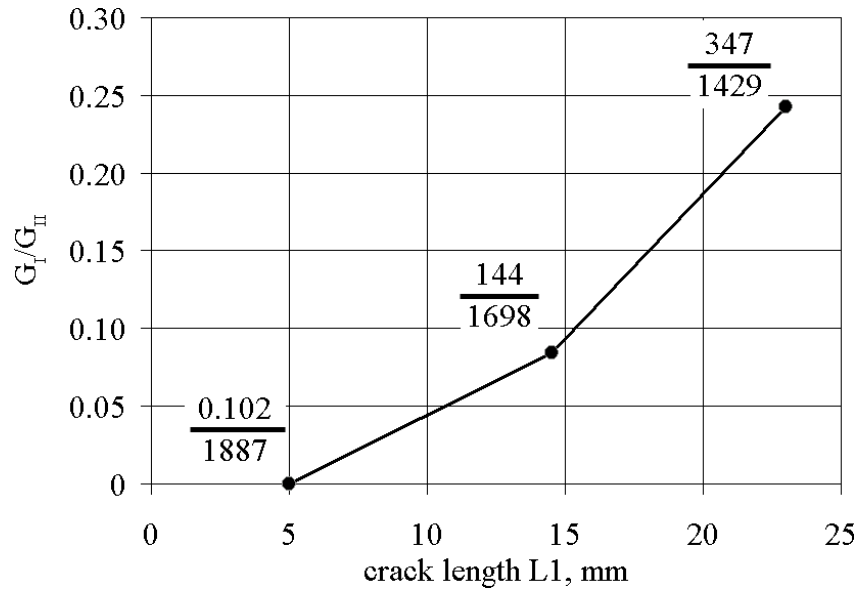


Figure 21.  $G_I/G_{II}$  ratios during crack growth for EP-1, standard case (1 mm lateral displacement, no L2 and L3, material properties adjusted to experimental fiber volume content).

## 5. CONCLUSIONS

The experimental results show significant differences between infusion resins for standard delamination tests and delamination at ply drops with the complex structured coupon. Results from both types of tests show the same trend from greatest delamination resistance to poorest: pDCPD, epoxy EP-1, toughened vinyl ester VE-2, vinyl ester VE-1 and polyester UP-1. The results indicate trade-offs between resin toughness and geometric refinement (such as number of plies dropped in a local area), which could impact blade design choices such as steepness of thickness tapering. The fatigue results were consistent with static results in terms of resin and geometric effects. Simulations of static damage growth vs. load, based on measured ply properties adjusted for fiber content and delamination test data, are in general agreement with experimental data for coupons containing ply drops. The simulations indicate sensitivity to several test and materials parameters. The findings of this study may be useful in resin selection and geometric design, as well as and manufacturing choices and structural integrity and reliability.

## 6. ACKNOWLEDGEMENTS

This research was supported in part by the Air Force Materials Laboratory through DEPSCoR, and Sandia National Laboratories.

## 7. REFERENCES

1. Mandell, J.F., Samborsky, D.D., Pancasatya, A., Sears, A.T. and Wilson, T.J., "Analysis of SNL/MSU/DOE Fatigue Database Trends for Wind Turbine Blade Materials." *Sandia National Laboratories Contractor Report* (in review, available on [www.coe.montana.edu/composites](http://www.coe.montana.edu/composites)).
2. Agastra, P., Samborsky, D. D. & Mandell, J. F. *50th AIAA/ASME/ASCE/AHS/ASC Structures, Structural Dynamics, and Materials Conference, Paper AIAA 2009-2411*, Palm Springs, CA, May 2009.
3. Mandell, J.F., Samborsky, D.D. and Cairns, D.S., "Fatigue of Composite Materials and Substructures for Wind Turbine Blades," *Contractor Report SAND2002-0771*, Sandia National Laboratories, Albuquerque, NM, 2002.
4. De Charentenay, F.X., "Concluding Remarks on the Application of Fracture Mechanics to Composite Materials," *Application of Fracture Mechanics to Composite Materials*, K. Freidrich, ed., Elsevier, 1989.
5. Trethewey, B.R., Gillespie, J.W., Jr. and Wilkins., "Interlaminar Performance of Tapered Composite Laminates," *Proceedings of the American Society for Composites, Fifth Technical Conference*, June 11-14, 1990, p. 361.
6. Murri, G.B., Salpekar, S.A., and O'Brien, T.K., *Composite Materials: Fatigue and Fracture (Third Volume)*, ASTM STP 1110, T.K. O'Brien, Ed., American Society for Testing and Materials, Philadelphia, 1991, pp. 312-339.
7. Samborsky, D.D., Wilson, T.W., Agastra, P., and Mandell, J.F., *J. Sol. Energy Eng.*, 2008 130, paper 031001.
8. Cairns, D.S., Mandell, J.F., Scott, M.E., Maccagnano, J.Z., "Design Considerations for Ply Drops in Composite Wind Turbine Blades," *1997 ASME Wind Energy Symposium*, ASME/AIAA, AIAA-97-0953, 1997, pp. 197-208.
9. Mandell, J.F., Cairns, D.S., Samborsky, D.D., Morehead, R.B., and Haugen, D.J., *J. Sol. Energy Eng.*, 2003, 125, paper 009304.
10. Hunston, D.L., Moulton, R.J., Johnson, N.J., and Bascom, W.D., *Toughened Composites*, ASTM STP 937, Norman J. Johnson, Ed., American Society for Testing and Materials, Philadelphia, 1987, pp. 74-94.
11. Krugar, R., and Konig, M., *Composite Materials: Fatigue and Fracture*, ASTM STP 1285, E. A. Armanios, Ed., American Society for Testing and Materials, 1997, pp. 162-178.
12. Edgecombe, B. D., Cruce, C., Stephen, T, McCarthy, T., Mandell, J. F., Samborsky, D. D., Agastra, P. and Wetzel, K. K. , "Effects of a new, high-toughness infusion resin on the fatigue performance and defect-tolerance of glass composite laminates," *AWEA Windpower conference*, Dallas, May 2010.
13. Reeder, J. R., and Crews, J. H., Jr., "The Mixed Mode Bending Method for Delamination Testing," *AIAA Journal*, vol. 28, 1990, pp. 1270-1276.
14. Agastra, P., "Mixed Mode Delamination of Glass Fiber/Polymer Matrix Composite Materials", *Masters Thesis*, Chemical and Biological Engineering Department, Montana State University, 2003.
15. Raju, I.S., *Engineering Fracture Mechanics* 28:3, 1987, pp. 251-274.
16. Russell, A.J. and Street, K.N., *Toughened Composites*, ASTM STP 937, N. J. Johnston, Ed., American Society for Testing and Materials, Phil., 1987, pp. 275-294.

17. Johnson, W.S. and Mangalgi, P.D., *Toughened Composites*, ASTM STP 937, N. J. Johnston, Ed., American Society for Testing and Materials, Phil., 1987, pp. 295-315.
18. Wilson, T.J., "Modeling of In-Plane and Interlaminar Fatigue Behavior of Glass and Carbon Fiber Composite Materials," *MS Thesis*, Department of Mechanical Engineering, Montana State University, 2006.